THE JOURNAL OF PHYSICAL CHEMISTRY C
A JOURNAL OF THE AMERICAN CHEMICAL SOCIETY

pubs.acs.org/JPCC

Comment

Reply to "Comment on 'Orthorhombic Symmetry and Anisotropic Properties of Rutile TiO_2'"

Wojciech Lulka, Nevill Gonzalez Szwacki,* Piotr Fabrykiewicz, Izabela Sosnowska, François Fauth, Emmanuelle Suard, and Radosław Przeniosło

J. Phys. Chem. C **2023**, *127* (38), 19240−19249. DOI: 10.1021/acs.jpcc.3c04573
J. Phys. Chem. C **2026**, *130*. DOI: 10.1021/acs.jpcc.5c08786

Cite This: https://doi.org/10.1021/acs.jpcc.6c01057

Read Online

ACCESS | Metrics & More | Article Recommendations

INTRODUCTION

In the Comment by Leineweber,[1] the author questions our interpretation of the powder diffraction data reported in ref 2 and suggests that the observed reflection-dependent broadening should be described within a tetragonal rutile-type model (space group $P4_2/mnm$) using anisotropic microstrain broadening, rather than by invoking an intrinsic lowering of the TiO_2 crystal structure symmetry to the orthorhombic $CaCl_2$-type (space group *Pnnm*).

We acknowledge that anisotropic microstrain is a common feature in powder diffraction experiments and can indeed contribute to peak broadening. However, the key point is that anisotropic microstrain and intrinsic orthorhombicity are *not mutually exclusive*. In fact, for rutile-related oxides close to the shear instability associated with the rutile → $CaCl_2$-type transformation, residual microstress and microstrain are expected to couple to the same symmetry-breaking distortion mode and can, therefore, enhance the orthorhombic response rather than mimic it. Consequently, the existence of microstrain should not be used as an argument against an orthorhombic ground state. In the following, we clarify why the arguments raised in the Comment do not invalidate our conclusions.

ORTHORHOMBIC DISTORTION IN RUTILE TIO_2 IS SMALL BUT SYSTEMATIC

The conclusions of our crystal structure study of rutile, TiO_2[2] were based on the observation of the *hkl*-selective peaks' broadening observed in both neutron powder diffraction (NPD) patterns and synchrotron X-ray powder diffraction (SXRPD) patterns of commercial rutile samples. The results of Rietveld[3,4] refinements obtained with the parent tetragonal space group $P4_2/mnm$ were not as good as those obtained with the orthorhombic subgroup *Pnnm*. For orthorhombic symmetry, we have different lattice parameters $a \neq b$ as well as different oxygen ions' coordinates $(x, y, 0)$, where $x \neq y$. In this short reply we will compare the influence of both conditions, i.e., $a \neq b$ and $x \neq y$ on the quality of refinement of NPD data of TiO_2[2] as well as the similar rutile-type β-PbO_2 from our previous study.[5]

Following the notation from ref 2, we use the lattice parameters' degree of distortion r_{ab}:

$$r_{ab} = 2\frac{a-b}{a+b} \tag{1}$$

and the atomic positions' degree of distortion r_{xy}:

$$r_{xy} = 2\frac{x-y}{x+y}. \tag{2}$$

From Figure 2 in the Comment[1] one can see that for rutile samples studied in ref 2 the relative difference of oxygen coordinates' $r_{xy} \simeq 10^{-2}$, is about 10 times larger than the relative difference of the lattice parameters' $r_{ab} \simeq 10^{-3}$. The NPD and SXRPD refinements presented in Tables 5−8 in ref 2 showed that the best fit was obtained for the orthorhombic symmetry with a correlation of ($a > b$ and $x > y$) but the statistical errors of $x - y$ were relatively large. In this reply we present arguments that the result with $x > y$ is a robust effect which is not a small addition to the orthorhombic lattice parameters' distortion.

The magnitude of the distortion is small and this is consistent with the very small energy differences obtained in first-principles calculations between the orthorhombic and tetragonal structures.[2] However, the proximity of the two structures does not imply that the tetragonal model is the correct symmetry description; rather, it indicates that TiO_2 is located extremely close to the rutile/$CaCl_2$-type instability so that the orthorhombic distortion is intrinsically weak and produces only subtle diffraction signatures.

Thus, the subtlety of the experimental signatures should be regarded as a natural consequence of an *incipient but symmetry-breaking* orthorhombic ground state rather than as evidence against it. In such a near-critical regime, weak perturbations such as sample history, microstructure, or residual stress may influence the magnitude of the distortion, but they do not change its systematic character.

Received: February 16, 2026
Revised: April 2, 2026
Accepted: April 2, 2026

A central statement of the Comment[1] is that anisotropic peak broadening should be interpreted as anisotropic microstrain rather than as orthorhombic peak splitting. While we agree that anisotropic microstrain is a realistic physical effect, the conclusion that this necessarily implies a tetragonal average structure is not justified.

For materials close to structural instabilities, microstress-induced strain fields are expected to couple strongly to the order parameter of the symmetry-lowering transition. In rutile-related oxides, the rutile → $CaCl_2$-type distortion is associated with a shear instability, commonly described by a soft elastic constant $C' = \frac{1}{2}(C_{11} - C_{12})$ in the tetragonal phase. Therefore, even if microstrain exists, it acts in the same symmetry-breaking channel and is expected to promote, stabilize, or enhance the orthorhombic distortion. In this sense, microstrain is not an "alternative explanation" but rather a mechanism that can increase the experimentally detectable orthorhombic response.

This interpretation is consistent with first-principles studies of pressure-induced instabilities in rutile TiO_2, which indicate that the system lies unusually close to the rutile → $CaCl_2$-type shear instability and that the reported transformation pressures may vary substantially, with suggestions that the onset of the instability can occur at significantly lower pressures depending on experimental conditions and sample-dependent effects.[6] Early experimental observations by Nicol and Fong[7] indicated a possible transition at relatively low pressures (~2−3 GPa), but these results were not conclusive as to the nature of the resulting phase. In particular, there is no clear evidence that this orthorhombic phase corresponds to the α-PbO_2-type structure. Subsequent studies have also considered the possibility that the observed distortions may be related to a $CaCl_2$-type structure, although this assignment remains debated.[8]

Thus, the presence of microstrain is fully compatible with our interpretation and, in fact, provides additional physical support for the existence of an intrinsic orthorhombic distortion in rutile TiO_2 at ambient pressure.

REANALYSIS OF NEUTRON POWDER DIFFRACTION DATA OF TIO_2 AND β-PBO_2

We performed a set of new refinements of the NPD pattern of TiO_2 (sample S1) by using the program FullProf.[9] These fits were done with the fixed oxygen coordinates: $x = x_0 + \xi\Delta x$ and $y = x_0 - \xi\Delta x$, i.e., taken proportional to a deformation parameter, ξ, where x_0 is the coordinate refined in the tetragonal symmetry. The value of Δx:

$$\Delta x = \frac{1}{2} r_{xy} x_0 \tag{3}$$

is chosen to give the orthorhombic solution, i.e., the best fit quality for the deformation parameter $\xi = \pm 1$ (see also eqs 5 and 6 in ref 2). We have done two sets of NPD refinements. The first, labeled as "*a,b* free" with freely refined $a \neq b$, and the second, labeled as "$a = b$" in which we restrict the condition $a = b$. It means we turn off any *hkl*-dependent broadening and the unit cell shape is tetragonal, while we allow the coordinates $x \neq y$. In this type of refinements, labeled as "$a = b$", we pretend "not-to-see" the *hkl*-dependent broadening. This approach can be used for NPD patterns, where the instrumental resolution makes *hkl*-dependent broadening less visible. We tried similar fits with SXRPD patterns, but due to the scattering contributions of oxygen vs Ti or Pb, as well as due to the good angular resolution in SXRPD, it was not possible to provide a meaningful fit with the "$a = b$" model and only the "*a,b* free" model worked well.

In each of these refinements for selected values of ξ, the values of x and y were fixed, while the lattice parameters a, b and c, the peak width parameters, peak shape pseudo-Voigt parameters and background and $2\theta_0$ were freely refined. Our intention is to show how the fit quality indicator depends on ξ. For technical reasons, the χ^2 value decimal rounding in the FullProf output file gives coarse data, so we used another fit quality indicator labeled as "N-sigma of the goodness of fit (GOF)" as described in ref 10, which has a similar significance as χ^2 and is less rounded. For each value of ξ we show "N-sigma" in Figure 1. The fit quality

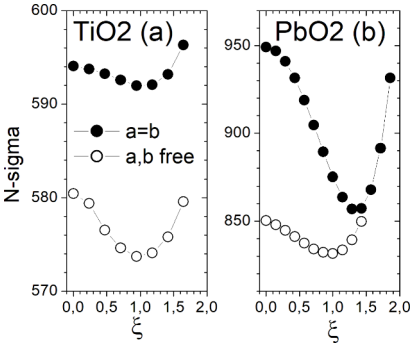

Figure 1. Results of fit quality for the NPD pattern of TiO_2 (a) and β-PbO_2 (b) measured at ambient conditions. The dependence of the fit quality indicator N-sigma (see text), is shown as a function of the deformation parameter ξ. The refinement done with free values of $a \neq b$ ("*a,b* free" open symbols) is compared with the refinement done in the restricted case $a = b$ ("$a = b$", solid symbols). Both models show a minimum near $\xi = 1$.

indicators obtained for *a,b* free are smaller than those obtained for the restricted $a = b$ model; however, both models show a $\chi^2(\xi)$ dependence with a minimum near $\xi = 1$ (see Figure 1). It means that even if we enforce the tetragonal shape to the unit cell, one gets a substantial improvement of the fit quality by allowing the oxygen coordinates to be different. In our earlier papers about TiO_2[2] and β-PbO_2,[5] the orthorombicity of the crystal structures was attributed to the peak asymmetry: due to $a \neq b$ the peak positions of *hkl* and *khl* are different and also due to $x \neq y$ the calculated contributions of *hkl* and *khl* are different. The successful fits assuming $a = b$ and $x \neq y$ are not related to peak asymmetry, and this effect is explained below.

CALCULATION OF PEAK INTENSITY VS DEFORMATION SIZE ξ

One needs to calculate the intensity contribution from *hkl* which is proportional to the square of the real structure factor $F(hkl)$ for the orthorhombic and centrosymmetric rutile structure. For $h + k + l$ even:

$$I \propto F(hkl)^2 = \{2f_M + 2f_O\{\cos[2\pi(hx + ky)] + \cos[2\pi(hx - ky)]\}\}^2 \tag{4}$$

For $h + k + l$ odd:

$$I \propto F(hkl)^2 = 4f_O{}^2\{\cos[2\pi(hx + ky)] - \cos[2\pi(hx - ky)]\}^2. \tag{5}$$

https://doi.org/10.1021/acs.jpcc.6c01057
J. Phys. Chem. C XXXX, XXX, XXX−XXX

For NPD f_M and f_O represent the coherent neutron scattering lengths of the metal ion and oxygen ion. For neutron scattering one gets $f_M = b(Ti) = -3.438$ fm (negative), $f_M = b(Pb) = 9.405$ fm and $f_O = b(O) = 5.803$ fm.[11] For SXRPD f_M and f_O represent the X-ray scattering factors for the respective ions.[12] In the parent tetragonal symmetry we take $x = y = x_0$ and the formulas 4 and 5 give the same values of $F(hkl)^2$ for the set of eight equivalent scattering vectors, namely for

$$(\pm h, \pm k, \pm l) \text{ and } (\pm k, \pm h, \pm l). \quad (6)$$

The contribution to the Bragg peak (hkl) intensity in the powder diffraction pattern is proportional to the sum of $F(hkl)^2$ calculated for the eight equivalent scattering vectors. We take $x = x_0 + \xi\Delta x$ and $y = x_0 - \xi\Delta x$, and we calculate the sum of all $F(hkl)^2$ for the eight equivalent scattering vectors from eq 6. The formula for the calculated intensity of the Bragg peak (hkl) in the powder diffraction pattern is expanded around x_0 in the small parameter $\xi\Delta x$. The odd power contributions from the expansion of cosines in eqs 4 and 5, coming from hkl and khl:

$$\sin[2\pi(h + k)x_0] \sin[2\pi(h - k)\Delta x\xi] + \sin[2\pi(h + k)x_0] \sin[2\pi(k - h)\Delta x\xi] \quad (7)$$

cancel each other and there are no terms of odd powers in $\xi\Delta x$. The calculated Bragg peak intensity in the powder diffraction pattern has a quadratic dependence on ξ:

$$I(hkl) = I_0(hkl) + D(hkl)\xi^2. \quad (8)$$

where $I_0(hkl)$ is the intensity calculated for the parent tetragonal structure. The intensities of peaks have been calculated by using FullProf. For the range of $\xi\Delta x$ of interest in this structure, the intensity changes due to the deformation ξ are of the order of 0.1% to 0.5%, as shown for representative peaks in Figures 2 and 3. This small effect leads, however, to an improvement of the fit quality with the $a = b$ restricted model. The sign of quadratic coefficient $D(hkl)$ depends on the specific hkl. Please note that for $h + k + l$ even, due to the negative sign of b(Ti) and the positive Ti^{4+} X-ray form-factor, the quadratic term $D(hkl)$ for NPD and SXRPD may have reversed signs for specific hkl; see Figure 2. For $h + k + l$ odd there are only the oxygen ions' term in eq 5 and the parabolic coefficients for NPD and SXRPD have the same sign.

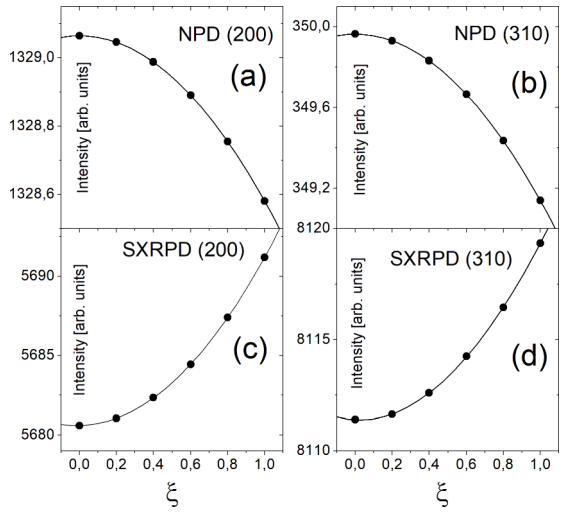

Figure 2. Calculated intensity for two representative Bragg peaks with $h + k + l$ even: (200) and (310), in the powder diffraction pattern of TiO_2 for NPD (a,b) and SXRPD (c,d). The lattice constants are restricted to $a = b$, but the oxygen coordinates' difference is given by the orthorhombic deformation parameter ξ (see text).

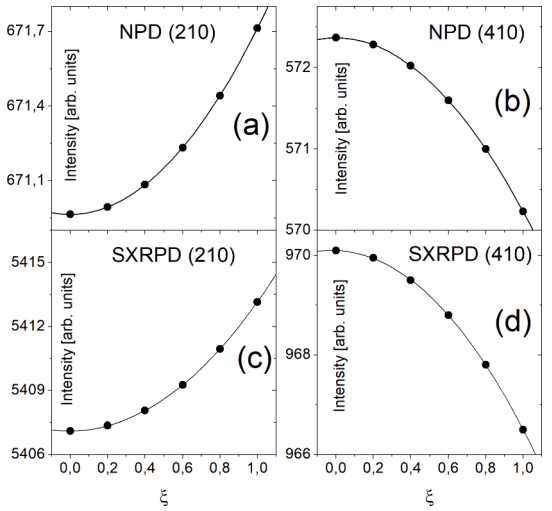

Figure 3. Calculated intensity for two representative Bragg peaks with $h + k + l$ odd: (210) and (410), in the powder diffraction pattern of TiO_2 for NPD (a,b) and SXRPD (c,d). The lattice constants are restricted to $a = b$, but the oxygen coordinates' difference is given by the orthorhombic deformation parameter ξ (see text).

As it was already shown by Leineweber[13] such a symmetry reduction down to orthorhombic gives a calculated powder diffraction pattern which is very similar to the pattern calculated by using the anisotropic peaks' broadening model proposed by Popa[14] and Stephens.[15] In the so-called Stephens formalism[14,15] it is assumed that there is a statistical distribution of the lattice parameters giving the peak widths hkl-dependence similar as that observed in the experimental data.[14,15] In the powder diffraction data refinements using the Stephens formalism, the atomic positions follow the restrictions of the parent symmetry (tetragonal $P4_2/mnm$); i.e., the Bragg peaks' intensities are calculated with oxygen ions located at $(x_0, x_0, 0)$, thus neglecting the effects of $x \neq y$.

ELASTIC ANISOTROPY OF ORTHORHOMBIC $CACL_2$-TYPE TIO_2 AND SNO_2

To further quantify the difference between the tetragonal and orthorhombic TiO_2 structure models, we analyze the elastic stiffness and compliance tensors for the orthorhombic (space group $Pnnm$) structure. The elastic stiffness tensor in Voigt notation is given by

$$\mathbf{C} = \begin{pmatrix} C_{11} & C_{12} & C_{13} & 0 & 0 & 0 \\ C_{12} & C_{22} & C_{23} & 0 & 0 & 0 \\ C_{13} & C_{23} & C_{33} & 0 & 0 & 0 \\ 0 & 0 & 0 & C_{44} & 0 & 0 \\ 0 & 0 & 0 & 0 & C_{55} & 0 \\ 0 & 0 & 0 & 0 & 0 & C_{66} \end{pmatrix}. \quad (9)$$

The compliance tensor is defined as

$$\mathbf{S} = \mathbf{C}^{-1}. \quad (10)$$

https://doi.org/10.1021/acs.jpcc.6c01057
J. Phys. Chem. C XXXX, XXX, XXX−XXX

Table 1. Elastic Stiffness Constants C_{ij} (GPa) for $CaCl_2$-Type (*Pnnm*) Structures[a]

Material	P	Code & method	Ref	C_{11}	C_{22}	C_{33}	C_{12}	C_{13}	C_{23}	C_{44}	C_{55}	C_{66}
SnO_2	0	VASP (PBE-PAW)	16	210.0	209.0	376.0	142.0	128.0	127.0	85.0	84.0	178.0
SnO_2	0	VASP (PBE-PAW)	17	215.4	215.1	388.6	147.2	134.6	133.1	86.3	86.5	181.0
SnO_2	5	VASP (PBE-PAW)	17	237.7	237.4	418.4	179.5	150.0	152.8	91.2	88.6	196.3
SnO_2	10	VASP (PBE-PAW)	17	281.8	225.0	448.4	214.4	189.5	161.2	95.3	95.5	210.4
TiO_2	0	QE (PBEsol-NC)	2	278.4	278.0	495.1	197.3	165.3	165.9	120.7	119.7	231.5
TiO_2	0	QE (rVV10-NC)	2	265.8	262.9	454.4	187.3	151.7	148.8	116.0	115.8	217.3

[a]P is the pressure in GPa. The column "Code & method" specifies the DFT implementation in the form *code* (*XC-pseudopotential*), where *XC* denotes the exchange−correlation functional and the pseudopotential label indicates the formalism used: PAW for the projector augmented-wave method (VASP) and NC for norm-conserving pseudopotentials (QUANTUM ESPRESSO).

Table 2. Compliance Tensor Components S_{ij} (TPa^{-1}) Obtained by Inversion of the Elastic Stiffness Tensor, $S = C^{-1}$, Using the Corresponding C_{ij} Values Listed in Table 1.

Material	P (GPa)	S_{11}	S_{22}	S_{33}	S_{12}	S_{13}	S_{23}	S_{44}	S_{55}	S_{66}
SnO_2	0	9.285	9.303	3.527	−5.521	−1.296	−1.263	11.765	11.905	5.618
SnO_2	0	9.218	9.178	3.452	−5.498	−1.310	−1.239	11.587	11.561	5.525
SnO_2	5	10.176	10.307	3.243	−6.989	−1.096	−1.258	10.965	11.287	5.094
SnO_2	10	13.581	16.400	3.162	−11.892	−1.464	−0.870	10.493	10.471	4.753
TiO_2	0	7.538	7.565	2.633	−4.810	−0.905	−0.929	8.285	8.354	4.320
TiO_2	0	7.891	7.928	2.822	−5.071	−0.974	−0.903	8.621	8.636	4.602

Table 3. Elastic Splittings (in %) Quantifying Deviations from Tetragonal Symmetry for the Stiffness (C) and Compliance (S) Tensors[a]

Material	P (GPa)	$\delta_{11}^{(C)}$	$\delta_{13}^{(C)}$	$\delta_{44}^{(C)}$	$\delta_{11}^{(S)}$	$\delta_{13}^{(S)}$	$\delta_{44}^{(S)}$	$\Delta\nu_{(2,1)\leftarrow 3}$
SnO_2	0	0.5	0.8	**1.2**	0.2	**2.6**	1.2	0.01
SnO_2	0	0.1	**1.1**	0.2	0.4	**5.5**	0.2	0.02
SnO_2	5	0.1	1.8	**2.9**	1.3	**13.8**	2.9	−0.05
SnO_2	10	**22.4**	16.1	0.2	18.8	**50.9**	0.2	0.19
TiO_2	0	0.1	0.4	**0.8**	0.4	**2.6**	0.8	−0.01
TiO_2	0	0.5	**1.9**	0.2	0.5	**7.6**	0.2	0.03

[a]The splittings δ_{11}, δ_{13}, and δ_{44} as well as the Poisson anisotropy measure $\Delta\nu_{(2,1)\leftarrow 3}$ are defined in eqs 11−14. Boldface marks the largest splitting within each tensor block (**C** or **S**) for a given material and pressure.

For a tetragonal crystal (point group $4/mmm$), the equalities $C_{11} = C_{22}$, $C_{44} = C_{55}$, and $C_{13} = C_{23}$ hold (and similarly for S_{ij}). To quantify deviations from tetragonal symmetry, we introduce the elastic splittings, analogous to the definitions of r_{ab} and r_{xy} (eqs 1 and 2)

$$\delta_{11} = 2\frac{|X_{11} - X_{22}|}{X_{11} + X_{22}} \tag{11}$$

$$\delta_{44} = 2\frac{|X_{44} - X_{55}|}{X_{44} + X_{55}} \tag{12}$$

and

$$\delta_{13} = 2\frac{|X_{13} - X_{23}|}{|X_{13}| + |X_{23}|} \tag{13}$$

where X_{ij} denotes either stiffness constants C_{ij} or compliance constants S_{ij}.

Table 1 summarizes the elastic stiffness constants C_{ij} (in GPa) for $CaCl_2$-type (*Pnnm*) SnO_2 and TiO_2 at selected pressures, while Table 2 lists the corresponding compliance tensor components (in TPa^{-1}). Table 3 provides elastic splittings δ_{11}, δ_{13}, and δ_{44} (in %) for both stiffness (**C**) and compliance (**S**) tensors. The results demonstrate that $CaCl_2$-type TiO_2 at ambient pressure is elastically extremely close to tetragonal symmetry (very small δ_{11} and δ_{44}, and moderate δ_{13} particularly in the compliance tensor). This quantitatively confirms that the orthorhombic distortion is intrinsically weak and that its diffraction fingerprints can naturally resemble those of a tetragonal phase affected by anisotropic broadening.

In addition, the last column of Table 3 reports the anisotropy of the Poisson response for uniaxial loading along the crystallographic direction [001]. Within linear elasticity, the Poisson ratio describing transverse strain along i induced by a uniaxial stress along j is given by $\nu_{ij} = -S_{ij}/S_{jj}$. We therefore define

$$\Delta\nu_{(2,1)\leftarrow 3} = \nu_{23} - \nu_{13} = \frac{S_{13} - S_{23}}{S_{33}} \tag{14}$$

which directly measures the deviation from tetragonal symmetry (for which $S_{13} = S_{23}$ and thus $\Delta\nu_{(2,1)\leftarrow 3} = 0$).

COMPARISON WITH OTHER RUTILE-RELATED OXIDES

The Comment[1] emphasizes that many rutile-related oxides exhibit a rutile → $CaCl_2$-type transition only under elevated pressure, and therefore TiO_2 should be tetragonal at ambient pressure. We stress that such general trends do not exclude the possibility that TiO_2 is already on the orthorhombic side of the instability at ambient conditions but with an exceptionally weak distortion. In this regime, the orthorhombic order parameter is

https://doi.org/10.1021/acs.jpcc.6c01057
J. Phys. Chem. C XXXX, XXX, XXX−XXX

expected to be small and can be influenced by sample microstructure, synthesis route, or residual stress, consistent with the variations observed for our two commercial powders.

Indeed, the pressure-driven structural instability of rutile TiO_2 has been discussed in the literature as occurring over a relatively broad and sometimes controversial pressure range, and it has been suggested that the transition could take place at significantly lower pressures depending on experimental conditions and sample-dependent effects.[6]

Furthermore, Tables 1−3 show that the orthorhombic elastic splittings in TiO_2 at ambient pressure are small but systematically nonzero, and comparable in magnitude to those in SnO_2 in the $CaCl_2$-type phase at low pressure. Importantly, the Poisson anisotropy measure $\Delta\nu_{(2,1)\leftarrow 3}$ is also finite for TiO_2, reflecting a measurable inequality between S_{13} and S_{23} and therefore a deviation from tetragonal symmetry. For SnO_2, the splittings increase significantly with pressure (e.g., at 10 GPa), reflecting the progressive stabilization of the $CaCl_2$-type distortion. This behavior supports the interpretation that TiO_2 at ambient pressure represents the limiting case of a $CaCl_2$-type orthorhombic phase with an exceptionally weak, but intrinsic symmetry-breaking distortion.

CONCLUSIONS

In summary, we agree that anisotropic microstrain broadening may contribute to powder diffraction peak shapes. However, we emphasize that microstrain does not exclude orthorhombicity. On the contrary, in a system close to a shear instability, microstress-induced microstrain is expected to couple to the same symmetry-breaking distortion and can enhance the orthorhombic response.

The fits of NPD data for TiO_2 and β-PbO_2 fully confirm the orthorhombic description of the crystal structure with the respective structural parameters published earlier in refs 2 and 5. In this short reply, we presented arguments supporting the importance of the oxygen ions' coordinate changes with positive r_{xy} as compared with the lattice parameter distortion only. The $\chi^2(\xi)$ (and N-sigma) dependence show clear minima near $\xi = 1$ both with ($r_{ab} > 0$) and without ($r_{ab} = 0$) lattice distortion. The validity of this approach is based on the expansion of the formulas for structure factors $F(hkl)^2$ in the rutile structure, which can be applied to other compounds, e.g., metal oxides MeO_2 or fluorides MeF_2.[18]

The $CaCl_2$-type distortion in rutile TiO_2 at ambient pressure is extremely small, which is quantitatively reflected in the elastic splittings of the orthorhombic stiffness and compliance tensors (Tables 1−3). Although the splittings δ_{11} and δ_{44} remain below the percent level, they are clearly nonzero, and the Poisson anisotropy measure $\Delta\nu_{(2,1)\leftarrow 3}$ also exhibits small nonzero values, demonstrating that the elastic response is not strictly tetragonal at ambient pressure.

AUTHOR INFORMATION

Corresponding Author

Nevill Gonzalez Szwacki − *Faculty of Physics, University of Warsaw, PL-02-093 Warsaw, Poland;* orcid.org/0000-0002-0518-844X; Phone: +48-22-55-32-797; Email: gonz@fuw.edu.pl

Authors

Wojciech Lulka − *Faculty of Physics, University of Warsaw, PL-02-093 Warsaw, Poland*

Piotr Fabrykiewicz − *Faculty of Physics, University of Warsaw, PL-02-093 Warsaw, Poland; Institute of Crystallography, RWTH Aachen University, D-52066 Aachen, Germany; Jülich Centre for Neutron Science at Heinz Maier-Leibnitz Zentrum, Forschungszentrum Jülich GmbH, D-85747 Garching, Germany;* orcid.org/0000-0001-7952-2466

Izabela Sosnowska − *Faculty of Physics, University of Warsaw, PL-02-093 Warsaw, Poland;* orcid.org/0000-0002-1574-7225

François Fauth − *CELLS-ALBA, ES-08290 Cerdanyola del Vallés, Barcelona, Spain;* orcid.org/0000-0001-9465-3106

Emmanuelle Suard − *Institut Laue-Langevin, FR-38042 Grenoble, France;* orcid.org/0000-0001-5966-5929

Radosław Przeniosło − *Faculty of Physics, University of Warsaw, PL-02-093 Warsaw, Poland;* orcid.org/0000-0002-7550-6976

Complete contact information is available at: https://pubs.acs.org/10.1021/acs.jpcc.6c01057

Notes

The authors declare no competing financial interest.

ACKNOWLEDGMENTS

We acknowledge the Polish Ministry of Education and Science for funding access to ILL by project no. 2023/WK/08. CELLS-ALBA is acknowledged for in-house beam time allocation of project ID 2020104796. The use of supercomputers at the Interdisciplinary Centre for Mathematical and Computational Modelling (ICM) at the University of Warsaw is also gratefully acknowledged.

REFERENCES

(1) Leineweber, A. Comment on "Orthorhombic Symmetry and Anisotropic Properties of Rutile TiO_2". *J. Phys. Chem. C* **2026**, DOI: 10.1021/acs.jpcc.5c08786.

(2) Gonzalez Szwacki, N.; Fabrykiewicz, P.; Sosnowska, I.; Fauth, F.; Suard, E.; Przeniosło, R. Orthorhombic Symmetry and Anisotropic Properties of Rutile TiO_2. *The Journal of Physical Chemistry C* **2023**, *127*, 19240−19249.

(3) van Laar, B.; Schenk, H. The development of powder profile refinement at the Reactor Centre Netherlands at Petten. *Acta Crystallogr., Sect. A* **2018**, *74*, 88−92.

(4) Rietveld, H. M. A profile refinement method for nuclear and magnetic structures. *J. Appl. Crystallogr.* **1969**, *2*, 65−71.

(5) Fabrykiewicz, P.; Przeniosło, R.; Gonzalez Szwacki, N.; Sosnowska, I.; Suard, E.; Fauth, F. Orthorhombic symmetry and anisotropic properties of PbO_2. *Physical Review B* **2021**, *103*, 064109.

(6) Montanari, B.; Harrison, N. M. Pressure-induced instabilities in bulk TiO_2 rutile. *Journal of Physics: Condensed Matter* **2004**, *16*, 273−292.

(7) Nicol, M.; Fong, M. Y. Raman Spectrum and Polymorphism of Titanium Dioxide at High Pressures. *The Journal of Chemical Physics* **1971**, *54*, 3167−3170.

(8) Mammone, J.; Nicol, M.; Sharma, S. Raman spectra of TiO_2-II, TiO_2-III, SnO_2, and GeO_2 at high pressure. *J. Phys. Chem. Solids* **1981**, *42*, 379−384.

(9) Rodriguez-Carvajal, J. Recent advances in magnetic structure determination by neutron powder diffraction. *Physica B* **1993**, *192*, 55−69.

(10) Ihringer, J. A quantitative measure for the goodness of fit in profile refinements with more than 20 degrees of freedom. *J. Appl. Crystallogr.* **1995**, *28*, 618−619.

(11) Sears, V. F. Neutron scattering lengths and cross sections. *Neutron News* **1992**, *3*, 26−37.

(12) Wilson, A. J. C., Ed. *International Tables for Crystallography, Volume C: Mathematical, Physical and Chemical Tables; International Tables for Crystallography*; Kluwer Academic Publishers: Dordrecht, Boston, London, 1992.
(13) Leineweber, A. Reflection splitting-induced microstrain broadening. *Powder Diffraction* **2017**, *32*, S35−S39.
(14) Popa, N. C. The (*hkl*) Dependence of Diffraction-Line Broadening Caused by Strain and Size for all Laue Groups in Rietveld Refinement. *J. Appl. Crystallogr.* **1998**, *31*, 176−180.
(15) Stephens, P. Phenomenological model of anisotropic peak broadening in powder diffraction. *J. Appl. Crystallogr.* **1999**, *32*, 281−289.
(16) Balakrishnan, K.; Veerapandy, V.; Fjellvåg, H.; Vajeeston, P. First-Principles Exploration into the Physical and Chemical Properties of Certain Newly Identified SnO_2 Polymorphs. *ACS Omega* **2022**, *7*, 10382−10393.
(17) Erdem, I.; Kart, H.; Cagin, T. High pressure phase transitions in SnO_2 polymorphs by first-principles calculations. *J. Alloys Compd.* **2014**, *587*, 638−645.
(18) Fabrykiewicz, P.; Przeniosło, R.; Sosnowska, I.; Fauth, F.; Oleszak, D. Verification of the de Wolff hypothesis concerning the symmetry of β-MnO_2. *Acta Crystallogr., Sect. A* **2019**, *75*, 889−901.

https://doi.org/10.1021/acs.jpcc.6c01057
J. Phys. Chem. C XXXX, XXX, XXX−XXX